Post-bifurcation equilibria in the plane-strain test of a hyperelastic rectangular block

N. Triantafyllidis [a,*], W.M. Scherzinger [a,b], H.-J. Huang [a]

[a] *Department of Aerospace Engineering, The University of Michigan, Ann Arbor, MI 48109-2140, USA*
[b] *Sandia National Laboratories, P.O. Box 5800, M.S. 0847, Albuquerque, NM 87185, USA*

Abstract

Of interest here is the bifurcated equilibrium solution of a homogeneous, hyperelastic, rectangular block under finite, plane-strain tension or compression. A general asymptotic analysis of the bifurcated equilibrium path about the principal solution's lowest critical load is presented using Lagrangian kinematics. The analysis is valid for any compressible hyperelastic material with axes of orthotropy aligned with the block's axes of symmetry in the reference (stress-free) configuration.

The general theory is subsequently applied to blocks of different constitutive laws. Results are presented in the form of bifurcated equilibrium branch's curvature at the critical load as function of the block's aspect ratio, since the sign of this curvature determines the branch's stability. For small aspect ratios there is agreement with existing structural models, while for relatively higher aspect ratios some rather counter-intuitive stability results appear, which strongly depend on the constitutive law.

© 2006 Elsevier Ltd. All rights reserved.

1. Introduction

The stability of prismatic solids subjected to axial loading is one of the oldest and most classical problems in structural mechanics. The first investigations by Euler on the buckling of axially compressed elastic columns (his celebrated ''*elastica*'') goes back about three centuries, while the initial investigations by Considère on the necking of bars subjected to axial tension are already more than a century old.

For a long time, the stability problems of prismatic solids were treated separately for compression and for tension, following the standard structural mechanics approach: the governing equations for the three-dimensional solid were approximated by one-dimensional (nonlinear) models, the examination of which yielded the sought stability results. For the technologically interesting case of axially compressed slender beams, their

---

* Corresponding author. Tel.: +1 734 763 2356; fax: +1 734 763 0578.
  E-mail address: nick@engin.umich.edu (N. Triantafyllidis).

critical load and mode is geometry-dominated and depends essentially on the form of the cross-section and on the boundary conditions, assuming that the solid's response is elastic up to critical strain levels. For the case of bars in tension, their stability is constitutive-dominated and depends essentially on the material response.

With the advent in the early 1950s of nonlinear continuum theories in solid mechanics, it was recognized that both compressive and tensile instabilities in prismatic bars can be treated within the same theoretical framework, i.e. as bifurcations from the constant stress principal configuration of the uniaxially loaded prismatic solid. The continuum mechanics-based (in two or three dimensions) bifurcation formulation of the axially loaded prismatic bar allows exact calculations of the problem at hand, which at the slender limit can be compared to structural approximations. Moreover, for the case of simple cross-sectional geometries (rectangular or cylindrical) analytical solutions are feasible.

The earlier bifurcation calculations for an axially compressed rectangular hyperelastic block in plane-strain are due to Levinson (1968) and Rivlin and Sawyers (1974), while the most general case is discussed in detail in the book by Ogden (1984). Subsequent investigations by Hill and Hutchinson (1975) for tension and by Young (1976) for compression, respectively, addressed the rectangular block's bifurcation problem for the more general case of incompressible, rate-independent solids. Moreover, the last two papers include an asymptotic analysis for the case of slender blocks, thus allowing comparison with corresponding, long-established, structural mechanics results.

Intimately linked to the bifurcation of solids is the determination of the post-bifurcated equilibrium paths and their stability. The pioneering work by Koiter (1945) has addressed this issue for elastic solids and provided general asymptotic techniques that allow the determination of the bifurcated equilibrium branches and their stability at the neighborhood of a critical point. Moreover, Koiter's general asymptotic methodology also addresses the issue of sensitivity to imperfections, thus linking the behavior of the idealized perfect solid to its real-life imperfect counterpart. A very readable review article on this topic for the case of simple eigenmodes is due to Budiansky (1974), while the general case of imperfect solids with multiple eigenmodes has been presented by Triantafyllidis and Peek (1992). Although it is not the approach followed here, it should also be mentioned at this point that the deeper reason for the existence of bifurcated solutions in the deformation of nonlinear solids is the loss of symmetries inherent in the corresponding boundary value problems. This approach started appearing in the more mathematically oriented mechanics literature from the 1970s and several stability problems have been examined from this viewpoint. The reader interested in this approach is referred to the work by Healey (1988) for a systematic treatment of the subject from a solid mechanics perspective.

As mentioned before, bifurcation studies, using two- and three-dimensional continuum mechanics formulations, have already been presented for the case of axially loaded prismatic solids. However (and perhaps due to the complexity of the required calculations), the general post-bifurcation analysis of this problem for arbitrary hyperelastic solids has not appeared in the literature – to the best of our knowledge – thus motivating the present work. It is worth noticing, that for the more complicated case of elastoplastic solids, numerical as well as asymptotic post-bifurcation analyses have been presented in the literature. The celebrated work by Shanley (1947) on the stability of the elastoplastic column should be mentioned at this point for the early works using the structural approach and the interested reader is referred to the review article by Hutchinson (1974) for more details on the post-bifurcation problem of elastoplastic solids using the continuum approach.

Of interest here is the post-bifurcation analysis of the axially loaded, homogeneous, compressible, hyperelastic rectangular block in plane-strain. The analysis is valid for any hyperelastic material with axes of orthotropy aligned with the axes of symmetry of the block in the reference (stress-free) configuration. More specifically, Section 2 presents, in full Lagrangian kinematics, the general asymptotic analysis giving the curvature of the bifurcated equilibrium branch, at the critical point, in the macroscopic strain vs bifurcation amplitude graph. According to general theory (e.g. see the review article of Budiansky (1974)) because of the symmetry of the boundary value problem and the uniqueness of the eigenmode, the sign of this curvature determines the branch's stability, with a positive curvature indicating a stable bifurcated equilibrium path in the neighborhood of the critical point.

In Section 3 are given the applications of the general theory for three different constitutive laws: compressible neo-Hookean, Gent (which exhibits strain saturation under tension) and Blatz–Ko (which exhibits stress saturation under tension). Following the determination of the block's critical load and eigenmode, the main

results of this work are presented at the end of Section 3 in the form of bifurcated branch's curvature at the critical load as a function of the block's aspect ratio. It is found that for small aspect ratios the results agree with existing structural models: initially stable bifurcated equilibrium paths for all materials under (bending-dominating) compression and initially unstable bifurcated equilibrium paths under tension for the Blatz–Ko solid (which exhibits a maximum force). For relatively higher aspect ratios some counter-intuitive results appear in compression, where depending on the constitutive law an unstable bifurcated equilibrium path can appear for relatively moderate aspect ratio blocks. A conclusion is presented in Section 4.

The lengthy analytical calculations required for the post-bifurcated asymptotic expansions about the principal solution's critical point are given in Appendix A. Appendix A also includes a section on the limit behavior of these asymptotic results for the case of slender blocks, thus allowing comparison with structural models.

2. Asymptotic analysis

This section pertains to the application of the general asymptotic theory of Lyapunov–Schmidt–Koiter (hereinafter referred to as LSK) to the determination of the initial post-bifurcation response of a hyperelastic rectangular block subjected to plane-strain (tensile or compressive) loading. The first subsection presents the principal solution and the general asymptotic expansions along the bifurcated equilibrium path of the load and the displacement field about the critical point. The last two subsections give the outline of the steps required for the determination of the first and second order coefficients in the bifurcated equilibrium path's asymptotic expansions. The corresponding detailed calculations are presented in Appendix A.

2.1. Principal solution and asymptotic expansions for bifurcated paths

The reference configuration of the solid under investigation is its stress-free configuration and the corresponding $2L_1 \times 2L_2$ rectangular block is shown in Fig. 1. The block which has an aspect ratio $r \equiv 2L_1/2L_2$ is loaded in the x_2 direction between two rigid, parallel, flat plates that cannot transmit shear, while the faces $x_1 = \pm L_1$ remain traction free.

The rectangular block is made of a hyperelastic, compressible material with a two-dimensional strain energy $W(I_1, I_2)$ (usually obtained from its three-dimensional counterpart under plane strain assumptions) where I_1 and I_2 are the two invariants of the right Cauchy–Green deformation tensor $\mathbf{C}$, namely
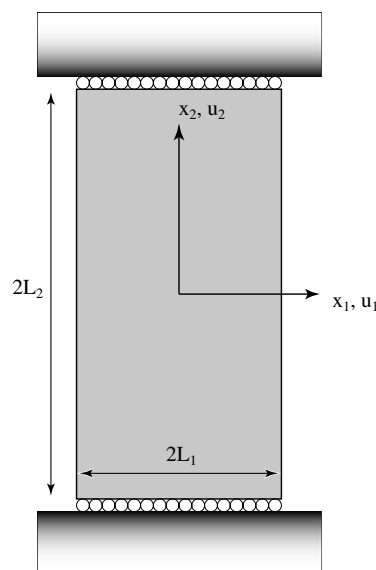

Fig. 1. Schematic representation of a rectangular block's plane-strain tension/compression test.

$$I_1 = C_{ii}, \quad I_2 = \det C_{ij}; \quad C_{ij} \equiv F_{ki}F_{kj}, \quad F_{ij} \equiv \delta_{ij} + u_{i,j} \tag{2.1}$$

with $u_i(x_1, x_2)$ the displacement components of a material point with reference configuration Cartesian coordinates x_i. In (2.1) are also recorded for completeness the definitions of right Cauchy–Green deformation tensor $\mathbf{C}$ and the deformation gradient tensor $\mathbf{F}$. Note the adoption in this paper of Einstein's summation convention over repeated Latin indexes, which range from 1 to 2, as well as the use of a comma followed by an index to denote partial differentiation with respect to the corresponding Cartesian coordinate, i.e. $f_i \equiv \partial f / \partial x_i$.

A displacement control test is considered, both in tension and in compression. The choice of a stiff loading device is dictated by the presence of a maximum force in the plane-strain tension test for some materials. Hence, the monotonically increasing with deformation "*load parameter*" $\Lambda(\Lambda \geqslant 0)$ is chosen to be the absolute value of the block's engineering strain (relative displacement of the two rigid end plates divided by their initial distance).

The potential energy $\mathcal{E}$ of the solid is a Λ-dependent functional of the displacement field u

$$\mathcal{E}(u, \Lambda) = \int_A W(I_1, I_2) \, \mathrm{d}A \tag{2.2}$$

with A denoting the reference domain of the solid. In addition to the smoothness conditions required for a finite potential energy $\mathcal{E}$, an admissible displacement field must also satisfy the essential boundary conditions

$$u_{2,1}(x_1, -L_2) = u_{2,1}(x_1, L_2) = 0; \quad u_1(0,0) = u_2(0,0) = 0; \quad |u_2(x_1, L_2) - u_2(x_1, -L_2)| = 2L_2\Lambda, \tag{2.3}$$

where the second set of constraints eliminate rigid body translations along x_i. For each load parameter Λ, defined as the average strain (absolute value) in the x_2 direction, the equilibrium displacement field is found by extremizing the solid's potential energy given in (2.2), i.e. by setting to zero the first functional derivative[1] of the potential energy with respect to the admissible displacement field

$$\mathcal{E}_{,u}(u, \Lambda)\delta u = 0. \tag{2.4}$$

One obvious solution to (2.4) is the "*principal solution*", denoted by $\overset{0}{u}(\Lambda)$, which corresponds to a constant strain equilibrium of the rectangular block and which is given in terms of the principal stretch ratios $\lambda_i(\Lambda)$ by

$$\overset{0}{u}_1(\Lambda) = [\lambda_1(\Lambda) - 1]x_1, \qquad \overset{0}{u}_2(\Lambda) = [\lambda_2(\Lambda) - 1]x_2. \tag{2.5}$$

The principal stretch ratios $\lambda_i(\Lambda)$ depend on the solid's constitutive response and the load parameter and are determined by

$$\Pi_1 = \frac{\partial W}{\partial \lambda_1} = 0, \qquad \lambda_2 = 1 \pm \Lambda, \tag{2.6}$$

where the first equation in (2.6) expresses the vanishing of the lateral first Piola–Kirchhoff stress Π_1 and thus gives λ_1 in terms of λ_2, while the second equation gives λ_2 in terms of the load parameter Λ (with sign $+$ for tension and sign $-$ for compression). To find the principal solution $\lambda_i(\Lambda)$, the invariants I_i of W in (2.6) must be expressed in terms of the principal stretch ratios

$$I_1 = (\lambda_1)^2 + (\lambda_2)^2, \qquad I_2 = (\lambda_1\lambda_2)^2. \tag{2.7}$$

Notice that in the absence of loading the displacement field vanishes $\overset{0}{u}(0) = 0$. For small values of the load parameter, the homogeneous principal solution is stable, i.e. it is also a minimizer of the potential energy satisfying $(\mathcal{E}_{,uu}\delta u)\delta u > 0$ for all nonzero admissible displacement fields δu. As Λ increases, it reaches a value Λ_c where the principal solution $\overset{0}{u}(\Lambda_c)$ is no longer a minimizer of the potential energy, but where the energy vanishes along a particular direction $\overset{1}{u}$, called the "*critical mode*" which satisfies the first equation in (2.8). At this

---

[1] Here and subsequently, $\mathcal{E}_{,u}v, (\mathcal{E}_{,uu}v)w, ((\mathcal{E}_{,uuu}v)w)z$, etc., denote, respectively, the first, second and third Frechet derivatives of the potential energy $\mathcal{E}$ with respect to u which are linear, bilinear and trilinear operators operating on admissible fields v, w and z and so on.

load, termed the "*critical load*", for the problem at hand a bifurcated equilibrium branch emerges with tangent $\overset{1}{u}$ from the principal solution. As shown in Triantafyllidis and Peek (1992), the presence of a bifurcated branch at the critical point is guaranteed by the second equation in (2.8)

$$\left(\mathcal{E}_{,uu}\left(\overset{0}{u}(\Lambda_c), \Lambda_c\right)\overset{1}{u}\right)\delta u = 0, \qquad \left(\mathcal{E}_{,u}\left(\overset{0}{u}(\Lambda_c), \Lambda_c\right)\overset{1}{u}\right) = 0. \tag{2.8}$$

For the axially loaded rectangular block problem at hand, the eigenmode $\overset{1}{u}$ of the bilinear stability operator $\mathcal{E}_{,uu}(\overset{0}{u}(\Lambda_c), \Lambda_c)$ is unique (up to a multiplicative scalar) and hence leads to a simple bifurcation at Λ_c.

Of interest in this work is the determination of the bifurcated equilibrium path emerging at Λ_c. Proving the existence of such a global bifurcated solution is a difficult and highly technical mathematical problem, which is beyond the scope of this work. It is therefore tacitly assumed that at the neighborhood of each critical point all the necessary conditions are met (essentially strong ellipticity and strong complementing boundary conditions), which allow for the existence of a bifurcated path (see Healey and Simpson (1998)). The bifurcated equilibrium path's displacement can be found analytically using the general LSK asymptotic expansion, (see Triantafyllidis and Peek (1992)) a power series of the "*bifurcation amplitude parameter*" ξ defined as the projection of bifurcated solution on the eigenmode

$$\xi \equiv \left\langle u - \overset{0}{u}, \overset{1}{u} \right\rangle, \tag{2.9}$$

where by $\langle u, v \rangle$ is denoted the inner product of two admissible displacement fields u and v. The choice presently adopted for the inner product is

$$\langle u, v \rangle \equiv \frac{1}{|A|} \int_A u_i v_i \, \mathrm{d}A \tag{2.10}$$

with the justification for this choice postponed for the results section. Here $|A|$ denotes the area of the reference domain A (and equals $4L_1L_2$). Finally, the unambiguous definition of the bifurcation amplitude in (2.9) requires fixing the norm of the eigenmode. Hence from here on

$$\left\langle \overset{1}{u}, \overset{1}{u} \right\rangle = 1. \tag{2.11}$$

According to the general theory presented in Triantafyllidis and Peek (1992), the LSK asymptotic expansion for the bifurcated equilibrium path about the critical point Λ_c is given by

$$u = \overset{0}{u}(\Lambda) + \xi\overset{1}{u} + \frac{\xi^2}{2}\overset{2}{u} + \mathrm{O}(\xi^3), \qquad \Lambda = \Lambda_c + \frac{\xi^2}{2}\Lambda_2 + \mathrm{O}(\xi^4). \tag{2.12}$$

Notice that the asymptotic expansion of Λ is in terms of even powers of ξ, due to the symmetry of the problem (it can be shown with the help of the eigenmode expressions (2.15) below that for all cases analyzed here $((\mathcal{E}^c_{,uuu}\overset{1}{u})\overset{1}{u})\overset{1}{u} = 0)$. The coefficients for the second order terms in the expansion of the displacement and the load parameter are:

$$\left(\mathcal{E}^c_{,uu}\overset{2}{u} + \left(\mathcal{E}^c_{,uuu}\overset{1}{u}\right)\overset{1}{u}\right)\delta v = 0, \quad \langle \delta v, \overset{1}{u} \rangle = 0,$$
$$\Lambda_2 = -\frac{1}{3}\frac{\left(\left(\left(\mathcal{E}^c_{,uuuu}\overset{1}{u}\right)\overset{1}{u}\right)\overset{1}{u}\right)\overset{1}{u} + 3\left(\left(\mathcal{E}^c_{,uuu}\overset{2}{u}\right)\overset{1}{u}\right)\overset{1}{u}}{\left((\mathrm{d}\mathcal{E}_{,uu}/\mathrm{d}\Lambda)^c\overset{1}{u}\right)\overset{1}{u}}, \tag{2.13}$$

where in the above equations the superscript $()^c$ denotes evaluation of the operator in question at the critical point $(\overset{0}{u}(\Lambda_c), \Lambda_c)$.

As shown in Triantafyllidis and Peek (1992), the stability of the bifurcated equilibrium path of the perfect block in the neighborhood of Λ_c depends on the sign of Λ_2; if $\Lambda_2 > 0$ the bifurcated path is stable, i.e. it minimizes the block's potential energy $\mathcal{E}$ in a neighborhood of the critical point, while for $\Lambda_2 < 0$ it is unstable near the critical point. Consequently according to Koiter's general theory, an imperfect block whose perfect counterpart has $\Lambda_2 < 0$ will exhibit a maximum average strain (recall that a displacement control is considered in the present analysis) lower than Λ_c and thus lead to a snap-through type instability. On the other hand, a

$\Lambda_2 > 0$ for the perfect block, guarantees a stable equilibrium path of its imperfect counterpart near Λ_c and hence allows average strain values exceeding Λ_c in a quasistatic loading process. The goal of the present paper is the calculation of Λ_2 for the rectangular block in tension and compression as a function of the aspect ratio r for different hyperelastic materials.

2.2. Critical load Λ_c and mode $\overset{1}{u}$

The determination of the critical load Λ_c and corresponding eigenmode $\overset{1}{u}$ for an arbitrary compressible hyperelastic rectangular block is given in Ogden (1984). However, for reasons of continuity of the presentation, the equations for these quantities are recorded here. More specifically, using the energy definition in (2.2), the rectangular block's eigenvalue problem in (2.8)$_1$ can be rewritten as

$$\int_A \left[L^c_{ijk\ell} \overset{1}{u}_{i,j} \delta u_{k,\ell} \right] \mathrm{d}A = 0, \qquad L^c_{ijk\ell} \equiv \frac{\partial^2 W\left(\overset{0}{u}(\Lambda_c)\right)}{\partial F_{ij} \partial F_{k\ell}}. \tag{2.14}$$

The solution of the resulting Euler–Lagrange differential equations and corresponding boundary conditions, leads (see Ogden (1984)) to the following expressions for the critical mode $\overset{1}{u}$:

$$\mathcal{S}^1 : \begin{cases} \overset{1}{u}_1 = v_1(x_1)\cos(p_2 x_2) - v_1(0) \\ \overset{1}{u}_2 = -v_2(x_1)\sin(p_2 x_2) \\ p_2 = n\pi/L_2 \end{cases}, \qquad \mathcal{A}^1 : \begin{cases} \overset{1}{u}_1 = v_1(x_1)\sin(p_2 x_2) \\ \overset{1}{u}_2 = v_2(x_1)\cos(p_2 x_2) - v_2(0) \\ p_2 = \left(n - \frac{1}{2}\right)\pi/L_2 \end{cases}, \tag{2.15}$$

where the symbols $\mathcal{S}^1$ and $\mathcal{A}^1$ designate the symmetric and antisymmetric, with respect to x_1, modes. Here n is an arbitrary integer (to be determined subsequently) while the detailed expressions for $v_i(x_1)$ are given in Appendix A. The critical load Λ_c depends on the material properties through $L^c_{ijk\ell}$, on the wavenumber n and on the aspect ratio r and the corresponding derivations are also recorded in Appendix A.

2.3. Second order terms Λ_2 and $\overset{2}{u}$

The calculation of Λ_2, required to determine the stability of the bifurcated equilibrium solution for the hyperelastic block, necessitates as an intermediate step the determination of the auxiliary displacement field $\overset{2}{u}$. To this end, from the general variational statement defining $\overset{2}{u}$ in (2.13)$_1$, one obtains

$$\int_A \left[\left(L^c_{ijk\ell} \overset{2}{u}_{k,\ell} + M^c_{ijk\ell mn} \overset{1}{u}_{k,\ell} \overset{1}{u}_{m,n} \right) \delta v_{i,j} \right] \mathrm{d}A = 0, \quad \left\langle \overset{1}{u}, \delta v \right\rangle = 0, \quad M^c_{ijk\ell mn} \equiv \frac{\partial^3 W\left(\overset{0}{u}(\Lambda_c)\right)}{\partial F_{ij} \partial F_{k\ell} \partial F_{mn}}. \tag{2.16}$$

Due to the symmetries of the problem and making use of (2.15), it can be shown that the solution of (2.16) results in the following expression for $\overset{2}{u}$

$$\overset{2}{u}_1 = w_1(x_1)\cos(2p_2 x_2) + \tilde{w}_1(x_1), \qquad \overset{2}{u}_2 = w_2(x_1)\sin(2p_2 x_2), \tag{2.17}$$

where the expressions for $w_i(x_1)$ and $\tilde{w}_1(x_1)$ are given in Appendix A.

Finally, the determination of Λ_2 from the general theory according to (2.13)$_3$ requires the calculation of the following quantities: The first term in the numerator of Λ_2 is found with the help of the energy definition in (2.2) to be

$$\left(\left(\left(\mathcal{E}^c_{,uuuu} \overset{1}{u}\right)\overset{1}{u}\right)\overset{1}{u}\right)\overset{1}{u} = \int_A \left[N^c_{ijk\ell mnpq} \overset{1}{u}_{i,j} \overset{1}{u}_{k,\ell} \overset{1}{u}_{m,n} \overset{1}{u}_{p,q} \right] \mathrm{d}A, \qquad N^c_{ijk\ell mn} \equiv \frac{\partial^4 W\left(\overset{0}{u}(\Lambda_c)\right)}{\partial F_{ij} \partial F_{k\ell} \partial F_{mn} \partial F_{pq}}. \tag{2.18}$$

The second term in the numerator of Λ_2 is found with the help of (2.2), and also from (2.13)$_1$ by substituting $\delta v = \overset{2}{u}$, to have the following two equivalent expressions:

$$\left(\left(\mathcal{E}^c_{,uuu} \overset{2}{u}\right)\overset{1}{u}\right)\overset{1}{u} = \int_A \left[M^c_{ijk\ell mn} \overset{2}{u}_{i,j} \overset{1}{u}_{k,\ell} \overset{1}{u}_{m,n} \right] \mathrm{d}A = -\int_A \left[L^c_{ijk\ell} \overset{2}{u}_{i,j} \overset{2}{u}_{k,\ell} \right] \mathrm{d}A. \tag{2.19}$$

Finally, the denominator of Λ_2 is also found with the help of the energy definition in (2.2) and the definition of tensor $\mathbf{M}$ in $(2.16)_3$ to be

$$\left((\mathrm{d}\mathcal{E}_{,uu}/\mathrm{d}\Lambda)^c \overset{1}{u} \right) \overset{1}{u} = \int_A \left[(\mathrm{d}L_{ijk\ell}/\mathrm{d}\Lambda)^c \overset{1}{u}_{i,j} \overset{1}{u}_{k,\ell} \right] \mathrm{d}A, \qquad (\mathrm{d}L_{ijk\ell}/\mathrm{d}\Lambda)^c = M^c_{ijk\ell mn} \left(\mathrm{d}\overset{0}{u}_{m,n}/\mathrm{d}\Lambda \right)^c. \tag{2.20}$$

The procedure for calculating Λ_c, $\overset{1}{u}$, $\overset{2}{u}$ and finally Λ_2 is detailed in Appendix A.

3. Results and discussion

The general theory of the previous section is hereby applied to specific materials. In the first subsection are introduced three different hyperelastic constitutive laws. The critical loads and modes of the corresponding rectangular blocks are presented in the second subsection. The third subsection gives the initial (i.e. at the critical load) curvature of the bifurcated equilibrium paths as function of the rectangular block's slenderness ratio for the different materials.

3.1. Material selection

Three different isotropic hyperelastic material models are used in the calculations presented here. The first model is a compressible neo-Hookean solid, which has the following energy density for plane-strain deformations

$$W(I_1, I_2) = \mu \left[\frac{1}{2} (I_1 - 2 - \ln I_2) + \frac{v}{1-v} (I_2^{1/2} - 1)^2 \right], \tag{3.1}$$

where μ and v are, respectively, the solid's shear modulus and plane-strain Poisson ratio at zero stress. As $v \to 1$ the material becomes incompressible, i.e. $I_2 \to 1$.

The second model, proposed by Gent (1996), is an experimentally based model for natural rubbers, with the following energy density for plane-strain deformations

$$W(I_1, I_2) = \mu \left[-\frac{J_m}{2} \ln \left(1 - \frac{I_1 - 2}{J_m} \right) - \frac{1}{2} \ln I_2 + \left(\frac{v}{1-v} - \frac{1}{J_m} \right) (I_2^{1/2} - 1)^2 \right], \tag{3.2}$$

where, in addition to the shear modulus μ and plane-strain Poisson ratio v, the material requires a third constant J_m which determines its locking strain in a uniaxial tension experiment. When $J_m \to \infty$, a simple calculation shows that the Gent solid in (3.2) reduces to the neo-Hookean solid in (3.1).

The third model, due to Blatz and Ko (1962), is based on experiments in compressible foam rubbers and has the following energy density in plane-strain

$$W(I_1, I_2) = \mu \left[\frac{1}{2} \frac{I_1}{I_2} + I_2^{1/2} - 2 \right], \tag{3.3}$$

The principal solution, i.e. the uniaxial plane-strain response of the rectangular block for the above introduced three different constitutive laws, is calculated with the help (2.6), (2.7) and the results are depicted in Fig. 2. More specifically the dimensionless Cauchy stress (σ_2/μ) versus logarithmic strain ($\ln \lambda_2$) under tension and compression is plotted in Fig. 2a. The dimensionless first Piola–Kirchhoff stress (Π_2/μ, which is the dimensionless force per unit width applied on the block) versus engineering strain ($\lambda_2 - 1$) under tension is plotted in Fig. 2b. The response of the compressible neo-Hookean, Gent (for $J_m = 50$) and Blatz–Ko solids with the same initial shear modulus (μ) and plane-strain Poisson ratio ($v = 1/3$) is plotted in solid lines, while the response of an almost incompressible neo-Hookean solid ($v = 50/51$) is plotted in dotted line. The choice of the specific value for the plane-strain Poisson ratio of the Gent and neo-Hookean solid ($v = 1/3$) is dictated by the value of this constant for the Blatz–Ko material (recall $v = -(\mathrm{d}\lambda_1/\mathrm{d}\lambda_2)_{\lambda_2=1}$).

Although near zero strain the response of the three compressible materials is the same, their finite strain behavior differs significantly. Notice from Fig. 2a that the Blatz–Ko solid has the stiffest response under compression, while the response of the compressible neo-Hookean and Gent solids (both with $v = 1/3$) is almost indistinguishable in the compressive range. In tension, the Gent solid has ultimately the stiffest response, while
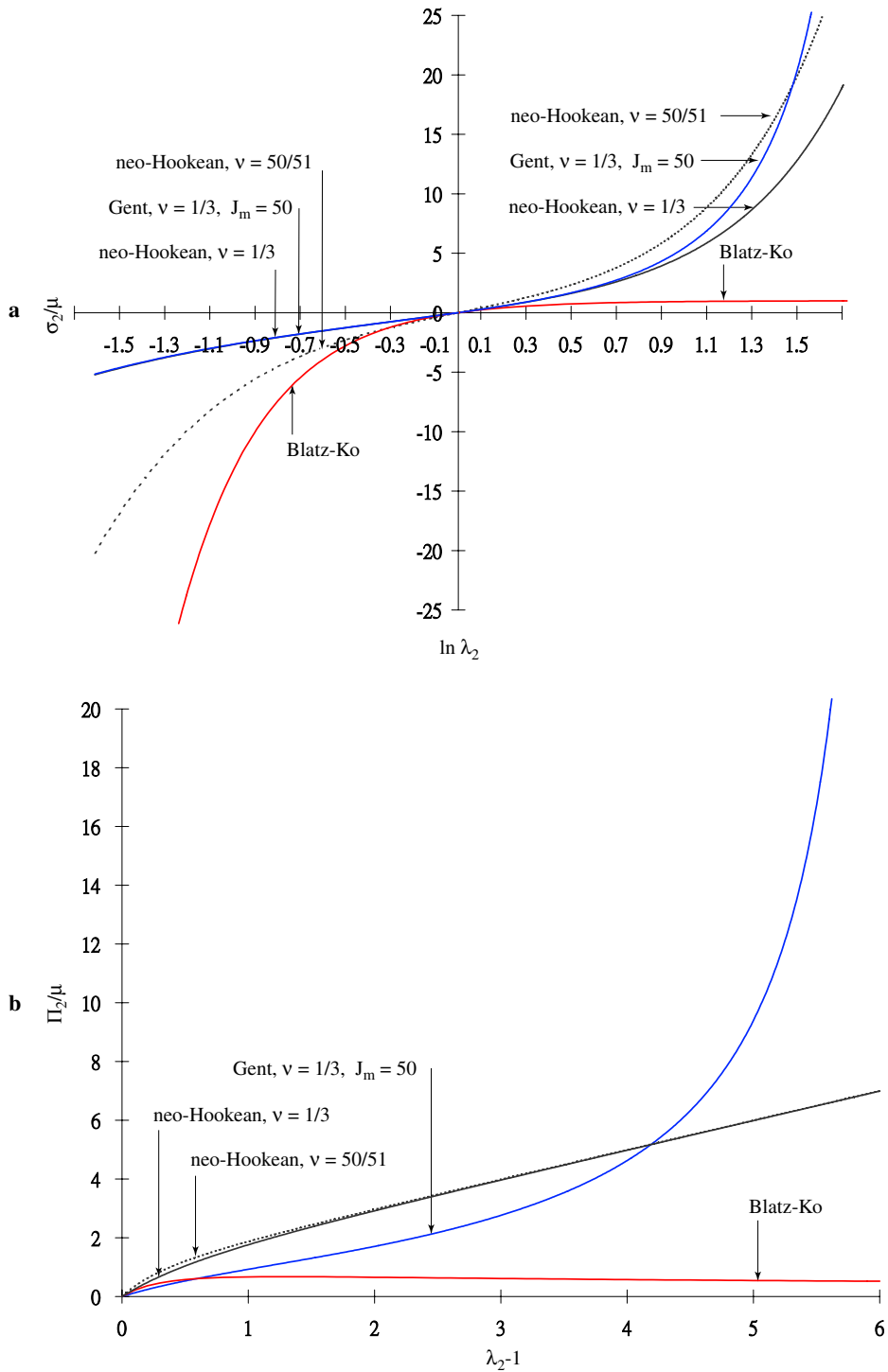
Fig. 2. In (a) is plotted the dimensionless Cauchy stress σ_2/μ vs logarithmic strain ϵ_2 of a rectangular block in tension and compression, while in (b) is plotted the dimensionless Kirchhoff stress Π_2/μ versus engineering strain $\lambda_2 - 1$ of the same block in tension. All four constitutive laws used have the same initial shear modulus μ, while in addition the Gent, the neo-Hookean for $v = 1/3$ and the Blatz–Ko materials share the same initial Poisson ratio $v = 1/3$.

the Blatz–Ko material is the softest and its Cauchy stress reaches an asymptote. The difference in the uniaxial response of the block under tension is better appreciated from Fig. 2b, which shows that for large strains, the force applied on the block behaves almost linearly for the neo-Hookean solid, shows strain locking (i.e. reaches an asymptote at a finite strain) for the Gent solid and has a maximum for the Blatz–Ko material at $\lambda_2 = 3^{0.75} \approx 2.28$.

A more fundamental difference between the above constitutive laws, is that while the neo-Hookean and Gent solids are rank one convex at all strains, the Blatz–Ko solid looses its rank one convexity at finite strains. In other words, the incremental equilibrium equations of the neo-Hookean and Gent are always strongly elliptic, while for the Blatz–Ko solid they exhibit real characteristics at finite strains (see Knowles and Sternberg (1975)). However, at the neighborhood of the critical load Λ_c all solids investigated here are shown to satisfy the strong ellipticity condition (a more detailed discussion on the ellipticity of the constitutive models is given in Appendix A). Assuming that the strong complementing boundary condition also holds in the same neighborhood (i.e. no surface bifurcations are possible in that vicinity), one expects the existence a bifurcated equilibrium branch emerging from the critical load Λ_c. The proof of this branch's existence requires sophisticated arguments of functional analysis and the interested reader is referred to Healey and Simpson (1998). The (assumed) existence of the bifurcated equilibrium branch emerging from the critical load makes possible the calculation of its curvature Λ_2 about the critical load Λ_c, which is the main goal of this work and is presented below in detail.

3.2. Critical loads and modes

The determination of the critical load as a function of the block's geometry for the above three constitutive laws, is presented in Figs. 3–6. More specifically, in Figs. 3 and 4 are plotted, for compression and tension, respectively, the lowest in absolute value bifurcation strains $(\lambda_2)_c - 1$ (i.e. the solutions of the bifurcation load
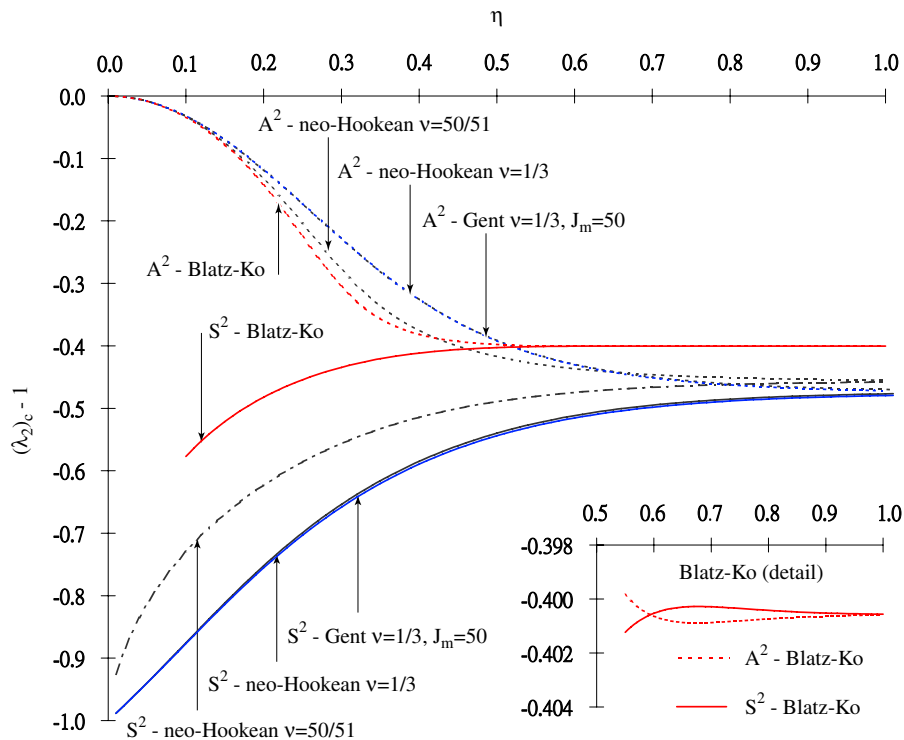

Fig. 3. Lowest bifurcation strain $(\lambda_2)_c - 1$ as a function of the dimensionless wave number η at the onset of bifurcation in a rectangular block under plane-strain compression for asymmetric and symmetric bifurcation modes for four different constitutive laws.
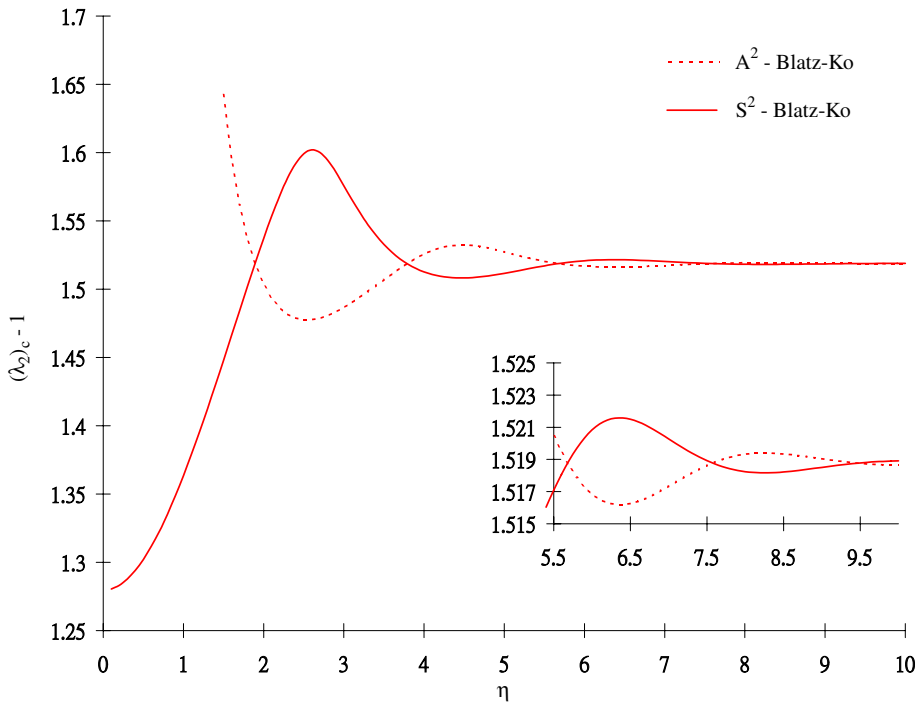
Fig. 4. Lowest bifurcation strain $(\lambda_2)_c - 1$ as a function of the dimensionless wave number η at the onset of bifurcation in a rectangular block under plane-strain tension for asymmetric and symmetric bifurcation modes for a Blatz–Ko material.
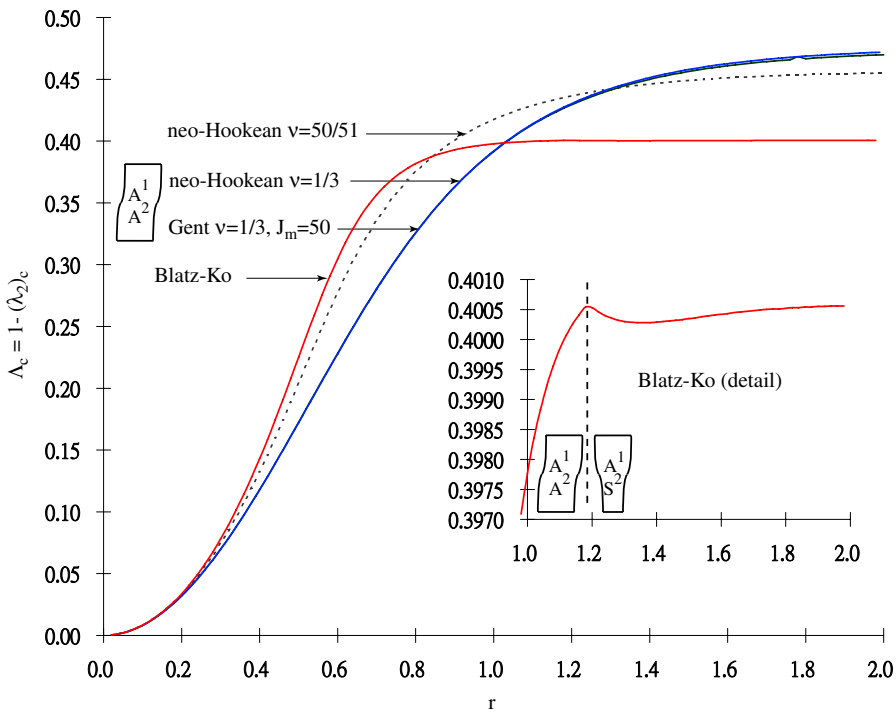

Fig. 5. Critical load Λ_c as a function of the block's aspect ratio r at the onset of bifurcation in a rectangular block under plane-strain compression for four different constitutive laws.

equations (A.6)), as functions of the geometric parameter η for the antisymmetric ($\mathcal{A}^2$) and symmetric ($\mathcal{S}^2$) cases. Based on these results, Figs. 5 and 6 record the critical loads Λ_c of the same blocks as functions of the slenderness ratios r. This two step approach is necessary to explain the discontinuities, due to mode changes, in some of the Λ_c vs r curves appearing in Figs. 5 and 6.

For all constitutive laws, the dependence of bifurcation strain $(\lambda_2)_c - 1$ on η in blocks under compression is presented in Fig. 3. Observe that for each constitutive law, the absolute value of the bifurcation strain increases (decreases) for the antisymmetric (symmetric) mode with increasing η, until they both reach the same asymptotic, material-dependent limit. At this limit, the bifurcation strain corresponds to a high wavenumber surface bifurcation of the half-space under compression, which is the only mode of instability possible for the stubby block. At the opposite end, the limit of a slender block ($\eta \to 0$) all antisymmetric mode curves go through zero, as expected from the vanishing buckling strain of a thin beam.

The bifurcation strains for the neo-Hookean and Gent solids are always monotonic functions of η. Moreover, there is a near coincidence between the bifurcation strains of the neo-Hookean and Gent solids that have the same plane-strain Poisson ratio $\nu = 1/3$, as expected from their almost identical response in compression, according to Fig. 2. In contrast to the neo-Hookean and Gent blocks, the antisymmetric and symmetric mode bifurcation strains for the Blatz–Ko block are no longer monotonic functions of η and cross each other, for the first time as η increases from zero, at $\eta \approx 0.6$. The monotonicity (nonmonotonicity) of the $(\lambda_2)_c - 1$ vs η curves is the reason for the monotonic (nonmonotonic) critical load Λ_c vs slenderness r curves of the different material blocks, as it will be subsequently discussed.

The dependence of the bifurcation strain $(\lambda_2)_c - 1$ on η for Blatz–Ko blocks under tension is presented in Fig. 4. As for the compression case, the bifurcation strain curves corresponding to antisymmetric (symmetric) modes reach the same asymptote, which corresponds to a surface instability of the Blatz–Ko half-space under tension. At the opposite end, the limit of a slender block ($\eta \to 0$) the symmetric mode curve goes through $(\lambda_2)_c = 3^{0.75}$, since the instability of a thin rod occurs at maximum force (see discussion of Fig. 2b). Again, as for the compressive case, the nonmonotonicity of the $(\lambda_2)_c - 1$ vs η curve is the reason for the nonmonotonic critical load Λ_c versus slenderness r curve of the Blatz–Ko block in tension.
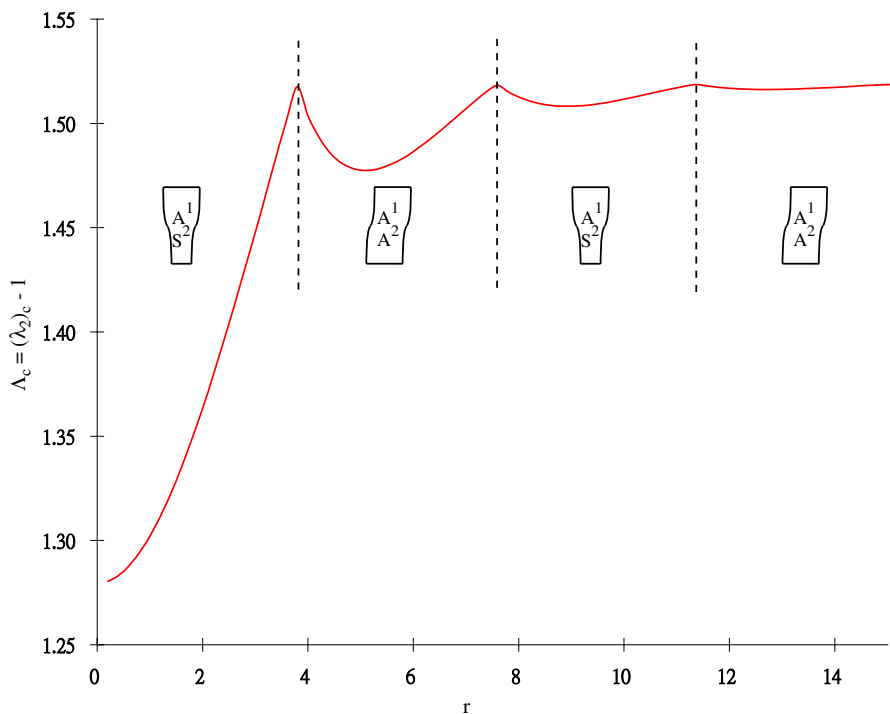

Fig. 6. Critical load Λ_c as a function of the block's aspect ratio r at the onset of bifurcation in a rectangular block under plane-strain tension for a Blatz–Ko material.

From the results in Figs. 3 and 4 one can find the critical load Λ_c vs slenderness r relations of the corresponding blocks by evaluating the bifurcation strain $(\lambda_2)_c - 1$ for $\eta = r/2, r, 3r/2, r, \ldots$ and then selecting the critical strain as the lowest absolute value $|(\lambda_2)_c - 1| = \Lambda_c$. If the minimum occurs for an η that is an integral (fractional) multiple of the block slenderness r, the corresponding critical mode is symmetric (antisymmetric) with respect to x_1, according to (2.15).

For the neo-Hookean and Gent blocks under compression, according to Fig. 3 the lowest strains always occur for the antisymmetric A^2 mode, whose monotonic dependence on η results in a minimum strain occurring at $\eta = r/2$ and hence in a monotonic Λ_c vs r dependence as seen in Fig. 5. The resulting critical mode has $n = 1$ and is antisymmetric with respect to both axes $(\mathcal{A}^1, \mathcal{A}^2)$. For the Blatz–Ko solid under compression, the critical mode for $r < 1.2$ is also antisymmetric with respect to both axes $(\mathcal{A}^1, \mathcal{A}^2)$, while for $r > 1.2$ it becomes symmetric with respect to x_2 axis $(\mathcal{A}^1, \mathcal{S}^2)$. The minimum strain always occurs at $\eta = r/2$ and hence the critical mode has $n = 1$. The change of mode, expected from the crossing of antisymmetric and symmetric bifurcation strain curves at $\eta \approx 0.6$ in Fig. 3, is reflected by the discontinuity of the critical load curve in Fig. 5 at $r \approx 1.2$.

For the Blatz–Ko blocks under tension according to Fig. 4, the minimum bifurcation strain occurs alternatively for symmetric or antisymmetric in x_2 modes but always for $\eta = r/2$, i.e. for the antisymmetric in x_1 mode. Consequently as seen in Fig. 6, the critical load Λ_c versus slenderness r curve is discontinuous and changes from an $(\mathcal{A}^1, \mathcal{S}^2)$ to an $(\mathcal{A}^1, \mathcal{A}^2)$ mode and back each time a discontinuity point is encountered as η increases from zero in Fig. 4.

The results in Figs. 5 and 6 give for a rectangular block with known material properties and aspect ratio, the critical load and corresponding eigenmode type, information required to calculate the curvature of the bifurcated equilibrium path at the critical point, as discussed next.

3.3. Curvature of the bifurcated equilibrium path

Having determined the critical load and corresponding eigenmode for a given block, the stage is set to calculate the curvature Λ_2 of the bifurcated equilibrium path about the critical load Λ_c. The various components required for the calculation of Λ_2 in (2.13)$_3$ are outlined in Section 2, while the full details are given in Appendix A.

To avoid numerical difficulties associated with slender blocks (i.e. when $r \ll 1$), all calculations reported here use as block dimensions $L_1 = 1$ and $L_2 = 1/r$. Evaluation of the curvature Λ_2 requires numerical integrations in the interval $[0, L_1]$. To this end the interval $[0, L_1]$ is divided into 10^4 equal subintervals. All integrations required in the x_1 direction use a simple trapezoidal rule based on this grid. The eigenmode $\overset{1}{u}$ and the second term in the post-bifurcation equilibrium displacement expansion $\overset{2}{u}$, which in turn requires the calculation of the auxiliary functions $w_i(x_1)$ defined in (A.13), are all evaluated on the same grid. Numerical experiments with denser grids on the interval $[0, L_1]$ gave almost identical results (errors of less than 10^{-4}). It is noteworthy that since all functions involved in the calculations of Λ_2 are separable – i.e. there are products of an x_1 function by a trigonometric x_2 function – the integrations in the $[0, L_2]$ interval are done analytically.

For the case of compression, the bifurcated equilibrium path's curvature at the critical load Λ_2/Λ_c versus the block's slenderness r is given in Fig. 7. Notice that, irrespective of the material properties, $\Lambda_2/\Lambda_c \to 3$ as $r \to 0$. From simple nonlinear beam models – such as Euler's elastica – it is expected that at the thin beam limit, the post-bifurcated behavior should be stable (i.e. $\Lambda_2 > 0$). What is rather surprising is that the curvature of the bifurcated equilibrium path at criticality is found to be independent of the constitutive law. A small-strain, moderate rotation structural beam model that accounts for axial compressibility (see Triantafyllidis (2006)) does indeed show that $\Lambda_2/\Lambda_c \to 3$ as $r \to 0$ when a displacement-based norm corresponding to (2.10) is adopted. Furthermore, this result is consistent with the asymptotic result of Budiansky (1974) for the axially compressed elastica (axial force asymptotics with respect to a slope-based norm are given in Budiansky (1974) – an asymptotic calculation of the elastica's end shortening is required in order to allow the successful comparison of the different slender beam models Triantafyllidis (2006)).

A rather surprising feature of the Λ_2/Λ_c vs r curves in Fig. 7 is that the post-bifurcated equilibrium solutions become unstable (i.e. $\Lambda_2 < 0$) for moderately stubby beams (at $r \approx 0.43$ for the Blatz–Ko block). The reason for this behavior is to be found in the moment-curvature relation for stubby beams. The post-buckling behavior of the thin beam under compression is stable since the increase in vertical displacement produces higher
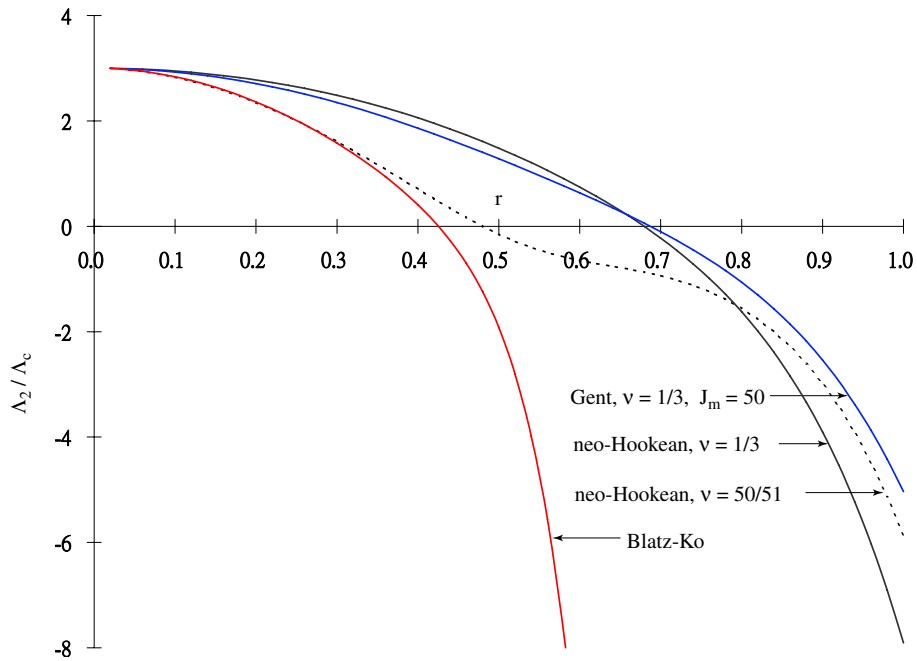
Fig. 7. Dimensionless curvature at critical load of the bifurcated equilibrium path Λ_2/Λ_c as a function of the block's aspect ratio r in a rectangular block under plane-strain compression for four different constitutive laws.

curvature at the end-sections which are compatible with the higher moments at these sections. As the beam becomes stubbier, the overall shortening of the beam in the bifurcated equilibrium solution, which results in a curvature increase at the end-sections is no longer sustainable because the moment, as a function of cur-
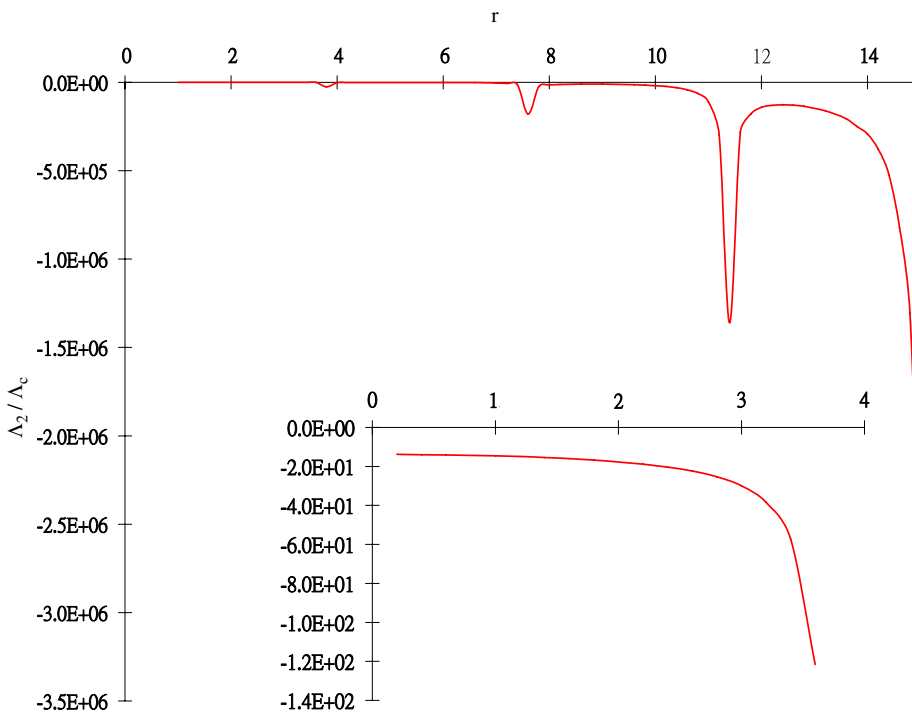

Fig. 8. Dimensionless curvature at critical load of the bifurcated equilibrium path Λ_2/Λ_c as a function of the block's aspect ratio r in a rectangular block under plane-strain tension for a Blatz–Ko material.

vature, reaches a maximum. The curvature at which a stubby beam reaches a maximum moment is material-dependent, thus explaining the different points on the r axis that the Λ_2/Λ_c curves cross for the different constitutive laws. Given that the Gent solid has the stiffest response, it is not surprising that it is the corresponding block that looses bifurcated path stability under compression at the highest aspect ratio ($r \approx 0.69$).

For the case of a Blatz–Ko block in tension, the bifurcated equilibrium path's curvature at the critical load Λ_2/Λ_c versus the block's slenderness r is given in Fig. 8. Notice that $\Lambda_2/\Lambda_c \to -27/2(3^{1/2} - 3^{-1/4})$ for the thin rod limit $r \to 0$. The unstable ($\Lambda_2 < 0$) bifurcated equilibrium path for the thin block under tension is expected since the block, having reached a maximum force at criticality, snaps back by developing a highly strained neck zone at one end while strains are lowered in the rest of its length. The unstable bifurcated path behavior near the critical load persists for any aspect ratio. The Λ_2/Λ_c vs r curve shows bumps near the regions where the Blatz–Ko block under tension changes eigenmodes at criticality, as seen by comparing Figs. 8 to 6.

The complex calculations leading to the evaluation of $\Lambda_2(r)/\Lambda_c(r)$ for arbitrary r need independent verification. To this end, and in addition to the asymptotic calculations done with MATHEMATICA for $r \to 0$, finite element (FEM) calculations for the rectangular elastic blocks are also performed with ABAQUS using slightly imperfect initial geometries. For the compressive case, blocks with a vertical mid–line at $x_1 = \zeta L_1 \sin(\pi x_2/L_2)$ (instead at $x_1 = 0$ for the perfect block) are considered, where the imperfection amplitude parameter $\zeta = 10^{-3}$, thus generating slightly asymmetric blocks in the shape of the relevant – near $r = 0$ – critical eigenmode in compression ($\mathcal{A}^1, \mathcal{A}^2$). Meshes of 20×40 bilinear quadrilateral elements (of equal sides $L_1/10$ and $L_2/20$ along x_1 and x_2) are used to calculate, with a help of a continuation method, the vertical displacement V_m versus the horizontal displacement H_m of the top mid-node. By changing the block's aspect ratio, one finds the value of the slenderness parameter r above which the V_m vs H_m curve reaches a maximum in V_m, thus indicating crossing of the r axis in the Λ_2/Λ_c curve in Fig. 7. This way it is possible to independently verify, with an 1% accuracy, the results of the corresponding calculations for the compressive case. Using the same mesh but a different initial geometry, i.e. a straight vertical axis but a slightly varying block thickness $2L_1 = 2L_1(1 + \zeta)$ $\sin(\pi x_2/L_2)$, imperfect block geometries are produced in the shape of the relevant – near $r = 0$ – critical eigenmode in tension ($\mathcal{A}^1, \mathcal{S}^2$). These FEM calculations using imperfect blocks, show unstable equilibrium paths past a maximum force, thus independently checking the validity of the stability results for the corresponding perfect block's bifurcated equilibrium paths.

4. Conclusion

The bifurcation and stability of axially loaded prismatic solids is a fundamental and much studied problem in solid mechanics, with the axially loaded rectangular block under plane-strain featuring preeminently among them. Although the onset of bifurcation for such a finitely strained block is well understood for a wide class of rate-independent solids, the hyperelastic block's post-bifurcation response has not been presented to-date, thus motivating the present work.

Using a Lyapunov–Schmidt–Koiter (LSK) expansion about the principal solution's lowest critical load, one can asymptotically construct the corresponding emerging bifurcated equilibrium branch. The sign of the curvature of this branch at the critical load, determines the branch's stability. The general theory is subsequently applied to three different constitutive laws: compressible neo-Hookean, Gent (which exhibits strain saturation under tension) and Blatz–Ko (which exhibits stress saturation under tension). The main results are presented in the form of bifurcated branch's curvature at the critical load as a function of the block's aspect ratio.

It is found that for small aspect ratios the results agree with existing structural models: initially stable bifurcated equilibrium paths for all materials under (bending-dominating) compression and initially unstable bifurcated equilibrium paths under tension for the Blatz–Ko solid (which exhibits a maximum force). Remarkably, at the slender block limit the curvature over critical load tends to a finite limit that – unlike the critical load itself – is independent of the block's constitutive law. Moreover, for relatively higher aspect ratios some counter-intuitive results appear in compression, where depending on the constitutive law an unstable bifurcated equilibrium path occurs for relatively moderate aspect ratio blocks, while for the Blatz–Ko blocks the bifurcated equilibrium paths are initially unstable for all aspect ratios investigated. The validity of the – rather

involved – analytical calculations in this work, is verified with asymptotic results for slender blocks and with finite element calculations for stubby blocks.

Acknowledgment

Appendix A

The calculation details for the bifurcation point and the asymptotic development of the bifurcated equilibrium path are given in this Appendix. More specifically, the derivations for the critical load Λ_c and eigenmode $\overset{1}{u}$ are given in the first subsection. The second order terms in the bifurcated equilibrium asymptotic expansions of the load Λ_2 and displacement $\overset{2}{u}$ are derived in the following subsection. Finally the limiting behavior of the asymptotic solution for small aspect ratios r is presented in the third subsection of the Appendix.

A.1. Calculation of Λ_c and $\overset{1}{u}$

The Euler–Lagrange differential equations of the eigenvalue problem, which result by a standard integration by parts of the variational equation (2.14), are given by:

$$
\begin{aligned}
L_{1111}^c \overset{1}{u}_{1,11} + L_{1122}^c \overset{1}{u}_{2,21} + L_{1212}^c \overset{1}{u}_{1,22} + L_{1221}^c \overset{1}{u}_{2,12} = 0, \\
L_{2112}^c \overset{1}{u}_{1,21} + L_{2121}^c \overset{1}{u}_{2,11} + L_{2211}^c \overset{1}{u}_{1,12} + L_{2222}^c \overset{1}{u}_{2,22} = 0
\end{aligned}
\tag{A.1}
$$

for any point in the reference domain $(-L_1 \leqslant x_1 \leqslant L_1, -L_2 \leqslant x_2 \leqslant L_2)$. The corresponding boundary conditions are:

$$
\begin{aligned}
L_{1111}^c \overset{1}{u}_{1,1} + L_{1122}^c \overset{1}{u}_{2,2} = 0, \quad & L_{2112}^c \overset{1}{u}_{1,2} + L_{2121}^c \overset{1}{u}_{2,1} = 0, \quad (x_1 = \pm L_1), \\
\overset{1}{u}_{1,2} = 0, \quad & \overset{1}{u}_{2,1} = 0, \quad (x_2 = \pm L_2),
\end{aligned}
\tag{A.2}
$$

where the first three equations are natural boundary conditions, while the last results from the kinematic admissibility condition (2.3). The orthotropy of the incremental moduli tensor **L** with respect to coordinate axes is used in the derivation of the above equations. The nonzero components of the incremental moduli evaluated on the principal branch according to (2.14)$_2$, are found with the help of (2.1) and (2.7) to be:

$$
\begin{aligned}
L_{1111}^c &= 4(\lambda_1)^2[W_{,11} + 2(\lambda_2)^2 W_{,12} + (\lambda_2)^4 W_{,22}] + 2[W_{,1} + (\lambda_2)^2 W_{,2}], \\
L_{2222}^c &= 4(\lambda_2)^2[W_{,11} + 2(\lambda_1)^2 W_{,12} + (\lambda_1)^4 W_{,22}] + 2[W_{,1} + (\lambda_1)^2 W_{,2}], \\
L_{1122}^c &= L_{2211}^c = 4\lambda_1\lambda_2[W_{,11} + ((\lambda_1)^2 + (\lambda_2)^2)W_{,12} + (\lambda_1\lambda_2)^2 W_{,22} + W_{,2}], \\
L_{1212}^c &= L_{2121}^c = 2W_{,1}, \\
L_{1221}^c &= L_{2112}^c = -2\lambda_1\lambda_2 W_{,2},
\end{aligned}
\tag{A.3}
$$

where use is made of the notation $W_{,i} \equiv \partial W / \partial I_i$ and $W_{,ij} \equiv \partial^2 W / \partial I_i \partial I_j$. It has been shown (see Ogden (1984)) that the above system of differential equations with constant coefficients has separable (in x_1 and x_2) solutions of the form given in (2.15). The mode's x_1 dependence is recorded below by giving the expressions for $v_i(x_1)$. Two cases $\mathcal{S}^2$ and $\mathcal{A}^2$ are distinguished, according to the symmetry or antisymmetry of the mode with respect to the x_2 axis:

$$\mathcal{S}^2 : \begin{cases} v_1(x_1) & = A_\alpha \sinh(\alpha p_2 x_1) + A_\beta \sinh(\beta p_2 x_1) \\ v_2(x_1) & = A_\alpha K(\alpha) \cosh(\alpha p_2 x_1) + A_\beta K(\beta) \cosh(\beta p_2 x_1) \\ A_\beta & = -\dfrac{(L^c_{1111}\alpha - L^c_{1122}K(\alpha)) \cosh(\alpha p_2 L_1)}{(L^c_{1111}\beta - L^c_{1122}K(\beta)) \cosh(\beta p_2 L_1)} A_\alpha \end{cases},$$

$$\mathcal{A}^2 : \begin{cases} v_1(x_1) & = B_\alpha \cosh(\alpha p_2 x_1) + B_\beta \cosh(\beta p_2 x_1) \\ v_2(x_1) & = B_\alpha K(\alpha) \sinh(\alpha p_2 x_1) + B_\beta K(\beta) \sinh(\beta p_2 x_1) \\ B_\beta & = -\dfrac{(L^c_{1111}\alpha - L^c_{1122}K(\alpha)) \sinh(\alpha p_2 L_1)}{(L^c_{1111}\beta - L^c_{1122}K(\beta)) \sinh(\beta p_2 L_1)} B_\alpha \end{cases}, \qquad (A.4)$$

$$K(x) \equiv [L^c_{1111}x^2 - L^c_{1212}]/[(L^c_{1122} + L^c_{1221})x], \quad (x = \alpha, \beta).$$

The constants α and β entering (A.4) are related to the roots of the (biquadratic) characteristic equation of the system of differential equations (A.1), namely:

$$ay^4 + 2by^2 + c = 0; \quad y = \pm i\alpha, \quad \pm i\beta, \qquad (A.5)$$

$$a \equiv L^c_{1111}L^c_{2121}, \quad 2b \equiv L^c_{1111}L^c_{2222} + L^c_{1212}L^c_{2121} - (L^c_{1122} + L^c_{2112})^2, \quad c \equiv L^c_{2222}L^c_{1212}.$$

Since the bifurcated solutions of interest are in the elliptic regime of the material response, the characteristic equation (A.5) evaluated at the critical load cannot have real solutions and hence $a > 0, c > 0, b > -\sqrt{ac}$. The solution has $\alpha, \beta \in \mathcal{R}$ if $b > \sqrt{ac}$, in which case the material is in the EI regime (elliptic-imaginary case since the roots of (A.5) are purely imaginary $\pm i\alpha, \pm i\beta$). When $|b| < \sqrt{ac}$, the material is in the EC regime (elliptic-complex case since the roots of (A.5) are complex conjugate $\delta \pm i\gamma$ – i.e. $(\alpha,\beta) = (\gamma + i\delta, \gamma - i\delta)$). It should also be noted that the eigenmode components $v_i(x_1)$ are always real, since for the EC regime $\beta = \bar{\alpha}$ and $A_\beta = \overline{A_\alpha}, B_\beta = \overline{B_\alpha}$ (remark is obvious for the EI regime since $\alpha, \beta \in \mathcal{R}$).

Substituting (A.4) into the boundary conditions (A.2) and using (A.1) and (A.5), one finds that one of the following equations must be satisfied at the critical load:

$$\left[\frac{\tanh(\pi\alpha\eta)}{\tanh(\pi\beta\eta)}\right]^{\varepsilon_2} = \frac{\alpha}{\beta}\left[\frac{\beta^2 - \chi}{\alpha^2 - \chi}\right], \quad \text{EI case, } (\alpha,\beta) = [(b \pm (b^2 - ac)^{1/2})/a]^{1/2},$$

$$\frac{\sinh(2\pi\gamma\eta)}{\sin(2\pi\delta\eta)} = \varepsilon_2 \frac{\gamma}{\delta}\left[\frac{\chi - \gamma^2 - \delta^2}{\chi + \gamma^2 + \delta^2}\right], \quad \text{EC case, } (\gamma,\delta) = [((ac)^{1/2} \pm b)/2a]^{1/2}, \qquad (A.6)$$

$$\eta \equiv p_2 L_1/\pi = nr \quad \text{or} \quad (n - 1/2)r, \quad \chi \equiv \frac{[L^c_{2222}(L^c_{1212}L^c_{2121} - (L^c_{1221})^2)]}{[L^c_{2121}(L^c_{1111}L^c_{2222} - (L^c_{1122})^2)]},$$

where $\varepsilon_2 = +1$ for the $\mathcal{S}^2$ type modes and $\varepsilon_2 = -1$ for the $\mathcal{A}^2$ type modes in (A.4). The critical load Λ_c for a given block, i.e. for a given energy density W and aspect ratio r, is the minimum nontrivial root of the two equations in (A.6), where the minimum is taken over all integers n and for $\varepsilon_2 = \pm 1$.

A.2. Calculation of Λ_2 and $\overset{2}{u}$

The Euler–Lagrange differential equations for $\overset{2}{u}$, found from the variational equation (2.16) using integration by parts, are:

$$
\begin{aligned}
L^c_{1111}\overset{2}{u}_{1,11} + (L^c_{1122} + L^c_{1221})\overset{2}{u}_{2,12} + L^c_{1212}\overset{2}{u}_{1,22} = &-[(M^c_{111111}(\overset{1}{u}_{1,1})^2 + 2M^c_{111122}\overset{1}{u}_{1,1}\overset{1}{u}_{2,2} \\
&+ M^c_{112222}(\overset{1}{u}_{2,2})^2 + M^c_{111212}(\overset{1}{u}_{1,2})^2 + M^c_{112121}(\overset{1}{u}_{2,1})^2 + 2M^c_{112112}\overset{1}{u}_{1,2}\overset{1}{u}_{2,1})_{,1} \\
&+ 2(M^c_{121112}\overset{1}{u}_{1,1}\overset{1}{u}_{1,2} + M^c_{121121}\overset{1}{u}_{1,1}\overset{1}{u}_{2,1} + M^c_{122212}\overset{1}{u}_{2,2}\overset{1}{u}_{1,2} + M^c_{122221}\overset{1}{u}_{2,2}\overset{1}{u}_{2,1})_{,2}], \\
L^c_{2121}\overset{2}{u}_{2,11} + (L^c_{2112} + L^c_{2211})\overset{2}{u}_{1,12} + L^c_{2222}\overset{2}{u}_{2,22} = &-[(M^c_{222222}(\overset{1}{u}_{2,2})^2 + 2M^c_{221122}\overset{1}{u}_{1,1}\overset{1}{u}_{2,2} \\
&+ M^c_{221111}(\overset{1}{u}_{1,1})^2 + M^c_{221212}(\overset{1}{u}_{1,2})^2 + M^c_{222121}(\overset{1}{u}_{2,1})^2 + 2M^c_{221221}\overset{1}{u}_{1,2}\overset{1}{u}_{2,1})_{,2} \\
&+ 2(M^c_{211112}\overset{1}{u}_{1,1}\overset{1}{u}_{1,2} + M^c_{211121}\overset{1}{u}_{1,1}\overset{1}{u}_{2,1} + M^c_{212221}\overset{1}{u}_{2,2}\overset{1}{u}_{2,1} + M^c_{212212}\overset{1}{u}_{2,2}\overset{1}{u}_{1,2})_{,1}],
\end{aligned}
\tag{A.7}
$$

for any point in the reference domain $(-L_1 \leqslant x_1 \leqslant L_1, -L_2 \leqslant x_2 \leqslant L_2)$. The corresponding boundary conditions are:

$$
\left.
\begin{aligned}
&L^c_{1111}\overset{2}{u}_{1,1} + L^c_{1122}\overset{2}{u}_{2,2} = -[M^c_{111111}(\overset{1}{u}_{1,1})^2 + 2M^c_{111122}\overset{1}{u}_{1,1}\overset{1}{u}_{2,2} \\
&+ M^c_{112222}(\overset{1}{u}_{2,2})^2 + M^c_{111212}(\overset{1}{u}_{1,2})^2 + 2M^c_{111221}\overset{1}{u}_{1,2}\overset{1}{u}_{2,1} + M^c_{112121}(\overset{1}{u}_{2,1})^2] \\
&L^c_{2112}\overset{2}{u}_{1,2} + L_{2121}\overset{2}{u}_{2,1} = -2[M^c_{211112}\overset{1}{u}_{1,1}\overset{1}{u}_{1,2} + M^c_{211121}\overset{1}{u}_{1,1}\overset{1}{u}_{2,1} \\
&+ M^c_{212221}\overset{1}{u}_{2,2}\overset{1}{u}_{2,1} + M^c_{212212}\overset{1}{u}_{2,2}\overset{1}{u}_{1,2}]
\end{aligned}
\right\}
\quad (x_1 = \pm L_1),
\tag{A.8}
$$
$$
\overset{2}{u}_{2,1} = 0, \quad \overset{2}{u}_{1,2} = 0, \quad (x_2 = \pm L_2),
$$

where the first three equations are natural boundary conditions while the last results from the kinematic admissibility condition (2.3). The components of rank six tensor **M**, defined in (2.16)$_3$, are calculated in a straightforward way with the help of (2.1) and (2.7), but due to the resulting cumbersome expressions will not be recorded here. The orthotropy of the principal solution implies that the only nonzero components of **M** are those containing an even number of similar indexes, just like the components of **L**. This property has been used in the derivations for $\overset{2}{u}$ presented here.

Substituting the eigenmode expressions of (2.15) into the system of (A.7) and (A.8) for the boundary value problem in $\overset{2}{u}$, one finds the x_2 dependence of $\overset{2}{u}$ recorded in (2.17). The x_1 dependence of $\overset{2}{u}$, i.e. the functions $w_1(x_1)$, $\tilde{w}_1(x_1)$ and $w_2(x_1)$, are obtained by introducing the expressions for $\overset{2}{u}$ in (2.17) into the governing differential equations (A.7)

$$
\begin{aligned}
&L^c_{1111}w''_1(x_1) + 2p_2(L^c_{1122} + L^c_{1221})w'_2(x_1) - (2p_2)^2 L^c_{1212}w_1(x_1) = -\varepsilon_1 E_1(x_1), \\
&L^c_{1111}\tilde{w}''_1(x_1) = -\tilde{E}'_1(x_1), \\
&L^c_{2121}w''_2(x_1) - 2p_2(L^c_{2211} + L^c_{2112})w'_1(x_1) - (2p_2)^2 L^c_{2222}w_2(x_1) = -\varepsilon_1 E_2(x_1),
\end{aligned}
\tag{A.9}
$$

$$
\begin{aligned}
E_1(x_1) \equiv &\tfrac{1}{2}[M^c_{111111}(v'_1)^2 - 2M^c_{111122}p_2 v'_1 v_2 + M^c_{112222}(p_2 v_2)^2 \\
&- M^c_{111212}(p_2 v_1)^2 - 2M^c_{111221}p_2 v_1 v'_2 - M^c_{112121}(v'_2)^2]' \\
&+ 2p_2[-M^c_{121112}p_2 v_1 v'_1 - M^c_{121121}v'_1 v'_2 + M^c_{122212}(p_2)^2 v_2 v_1 + M^c_{122221}p_2 v_2 v'_2], \\
\tilde{E}_1(x_1) \equiv &\tfrac{1}{2}[M^c_{111111}(v'_1)^2 - 2M^c_{111122}p_2 v'_1 v_2 + M^c_{112222}(p_2 v_2)^2 \\
&+ M^c_{111212}(p_2 v_1)^2 + 2M^c_{111221}p_2 v_1 v'_2 + M^c_{112121}(v'_2)^2], \\
E_2(x_1) \equiv &[-M^c_{211112}p_2 v'_1 v_1 - M^c_{211121}v'_1 v'_2 + M^c_{212212}(p_2)^2 v_1 v_2 + M^c_{212221}p_2 v_2 v'_2]' \\
&+ p_2[-M^c_{221111}(v'_1)^2 + 2M^c_{221122}p_2 v'_1 v_2 - M^c_{222222}(p_2 v_2)^2 \\
&+ M^c_{221212}(p_2 v_1)^2 + 2M^c_{221221}p_2 v_1 v'_2 + M^c_{222121}(v'_2)^2],
\end{aligned}
$$

where $\varepsilon_1 = +1$ for an $\mathcal{S}^1$ mode and $\varepsilon_1 = -1$ for an $\mathcal{A}^1$ mode, according to (2.15) and where the functions $v_i(x_1)$ are given by (A.4). Note that a symbol followed by a prime denotes ordinary differentiation with respect to x_1. Substitution of the eigenmode $\overset{2}{u}$ in (2.17) to the boundary conditions (A.8) yields:

$$\begin{cases} L_{1111}^c w_1' + 2p_2 L_{1122}^c w_2 = -\varepsilon_1 F_1 \\ L_{1111}^c \tilde{w}_1' = -\tilde{E}_1 \\ L_{2121}^c w_2' - 2p_2 L_{2112}^c w_1 = -\varepsilon_1 F_2 \end{cases} \quad (x_1 = \pm L_1), \tag{A.10}$$

$$F_1 \equiv \frac{1}{2}[M_{111111}^c (v_1')^2 - 2M_{111122}^c p_2 v_1' v_2 + M_{112222}^c (p_2 v_2)^2$$
$$- M_{111212}^c (p_2 v_1)^2 - 2M_{111221}^c p_2 v_1 v_2' - M_{112121}^c (v_2')^2],$$
$$F_2 \equiv -M_{211112}^c p_2 v_1 v_1' - M_{211121}^c v_1' v_2' + M_{212212}^c (p_2)^2 v_2 v_1 + M_{212221}^c p_2 v_2 v_2',$$

where the definitions of ε_1 and $v_i(x_1)$ are the same as for (A.9).

The determination of $\tilde{w}_1(x_1)$ from the differential equation (A.9) and boundary condition (A.10) is straightforward

$$\tilde{w}_1(x_1) = -\frac{1}{L_{1111}^c} \int_0^{x_1} \tilde{E}_1(y)\, dy, \tag{A.11}$$

where the constant of integration is fixed from the constraint against rigid body displacement in (2.3)$_2$.

Finding $w_i(x_1)$ is a considerably more complicated task which proceeds as follows: notice that the system of differential equations for $w_i(x_1)$ can be decoupled to yield:

$$a w_i''''(x_1) - 2b(2p_2)^2 w_i''(x_1) + c(2p_2)^4 w_i(x_1) = \varepsilon_1 \hat{E}_i(x_1), \quad (i = 1, 2), \tag{A.12}$$

$$\hat{E}_1(x_1) \equiv -E_1'' L_{2121}^c + E_2'(2p_2)(L_{1122}^c + L_{1221}^c) + E_1(2p_2)^2 L_{2222}^c,$$
$$\hat{E}_2(x_1) \equiv -E_2'' L_{1111}^c - E_1'(2p_2)(L_{2211}^c + L_{2112}^c) + E_2(2p_2)^2 L_{1212}^c,$$

where the definition of the constants a, b, c is given in (A.5). The solution to the above fourth order ordinary differential equations with constant coefficients is found, with the help of (A.9), to be:

$$w_1(x_1) = \hat{A}_\alpha \sinh(2\alpha p_2 x_1) + \hat{A}_\beta \sinh(2\beta p_2 x_1) + \varepsilon_1 \int_0^{x_1} G(x_1 - y)\hat{E}_1(y)\, dy,$$

$$w_2(x_1) = -[(\hat{A}_\alpha K(\alpha) + \varepsilon_1 J(\alpha))\cosh(2\alpha p_2 x_1) + (\hat{A}_\beta K(\beta) - \varepsilon_1 J(\beta))\cosh(2\beta p_2 x_1)] + \varepsilon_1 \int_0^{x_1} G(x_1 - y)\hat{E}_2(y)\, dy, \tag{A.13}$$

$$G(x_1) \equiv \frac{1}{a(2p_2)^3(\alpha^2 - \beta^2)}\left[\frac{\sinh(2\alpha p_2 x_1)}{\alpha} - \frac{\sinh(2\beta p_2 x_1)}{\beta}\right],$$

$$J(x) \equiv \frac{1}{(2p_2)^3 L_{1111}^c(\alpha^2 - \beta^2)}\left[\frac{K(x)}{x}E_1'(0) + \frac{2p_2}{x^2}E_2(0)\right], \quad (x = \alpha, \beta),$$

where the expression for $K(x)$ is defined in (A.4). It should be mentioned here that in deriving the above results with the help of (A.4), one notices that E_1, $\hat{E}_1$, F_2 and E_2, $\hat{E}_2$, F_1 defined in (A.9), (A.10) are odd and even functions respectively of their argument x_1. These properties imply from (A.9), (A.10) that w_1 and w_2 are in their turn odd and even functions, respectively, of x_1.

Using the above results for $w_i(x_1)$ into the corresponding boundary conditions in (A.10), one obtains a linear system for the two unknown constants $\hat{A}_\alpha$, $\hat{A}_\beta$, appearing in (A.13), as follows:

$$\begin{bmatrix} P_c(\alpha)\hat{A}_\alpha + P_c(\beta)\hat{A}_\beta = \varepsilon_1 Q_c \\ P_s(\alpha)\hat{A}_\alpha + P_s(\beta)\hat{A}_\beta = \varepsilon_1 Q_s \end{bmatrix}, \tag{A.14}$$

$$P_c(x) \equiv [L_{1111}x - L_{1122}K(x)]\cosh(2xp_2L_1), \quad (x = \alpha, \beta),$$

$$P_s(x) \equiv [L_{2121}xK(x) + L_{2112}]\sinh(2xp_2L_1), \quad (x = \alpha, \beta),$$

$$Q_c \equiv [L_{1122}[J(\alpha)\cosh(2\alpha p_2L_1) - J(\beta)\cosh(2\beta p_2L_1)] - \frac{F_1(L_1)}{2p_2}$$

$$- L_{1122}\int_0^{L_1} G(L_1 - y)\hat{E}_2(y)\,\mathrm{d}y - \frac{L_{1111}}{2p_2}\int_0^{L_1} G'(L_1 - y)\hat{E}_1(y)\,\mathrm{d}y,$$

$$Q_s \equiv -L_{2121}[\alpha J(\alpha)\sinh(2\alpha p_2L_1) - \beta J(\beta)\sinh(2\beta p_2L_1)] + \frac{F_2(L_1)}{2p_2}$$

$$- L_{2112}\int_0^{L_1} G(L_1 - y)\hat{E}_1(y)\,\mathrm{d}y + \frac{L_{2121}}{2p_2}\int_0^{L_1} G'(L_1 - y)\hat{E}_2(y)\,\mathrm{d}y.$$

Solution of the above system for $\hat{A}_\alpha$, $\hat{A}_\beta$ completes the determination of $w_i(x_1)$ and hence of $\overset{2}{u}$ according to (2.17). It can be shown that $w_i(x_1)$, $\tilde{w}_1(x_1)$ and consequently $\overset{2}{u}$ are always real functions (obvious for the EI regime and following in the EC regime from the fact that $\overline{\alpha} = \beta$, which implies $\hat{\overline{A}}_\alpha = \hat{A}_\beta$).

The determination of Λ_2 follows by substituting the above found functions $\overset{1}{u}$ and $\overset{2}{u}$ into (2.13)$_3$. All the required calculations for arbitrary values of the aspect ratio r, are based on a FORTRAN code written for this purpose.

A.3. Asymptotic behavior of thin blocks $r \to 0$

The asymptotic calculations for the thin block limiting case $(r \to 0)$ are based on the above presented analysis and use the symbolic manipulator program MATHEMATICA. Recall from the discussion of the initial post-bifurcation curvature results in Section 3 that the dimensions of the block are: $L_1 = 1$ and $L_2 = 1/r$ and that the eigenmode $\overset{1}{u}$ is normalized (see 2.11) using the inner product definition in (2.10). The results for compression are given first, followed by the results for tension.

(i) Compression (critical mode $\mathcal{A}^1$, $\mathcal{A}^2$; critical wavenumber $n_c = 1$)

The asymptotic expressions given below are valid for all three constitutive laws. For the neo-Hookean and Gent materials the value of Poisson ratio v is arbitrary, while for the Blatz–Ko material the corresponding expressions are valid for $v = 1/3$. The asymptotic expressions are given up to the lowest order in the slenderness ratio required for the calculation of Λ_2, the post-bifurcation curvature at the critical point.

To calculate Λ_2, one starts with the asymptotic expressions of the stretch ratios λ_i and $v_i(x_1)$ (the x_1-dependent part of the eigenmode $\overset{1}{u}$) at the critical point:

$$(\lambda_1)_c = 1 + \frac{v}{12}(\pi r)^2 + \mathrm{O}(r^4), \quad (\lambda_2)_c = 1 - \frac{1}{12}(\pi r)^2 + \mathrm{O}(r^4),$$

$$v_1(x_1) = \sqrt{2} + \mathrm{O}(r^2), \quad v_2(x_1) = -\frac{x_1}{\sqrt{2}}\pi r + \mathrm{O}(r^3). \tag{A.15}$$

The next piece of information needed are the asymptotic expansions for $w_i(x_1)$, $\tilde{w}_1(x_1)$ (the x_1-dependent parts of $\overset{2}{u}$) given below to their leading order in r

$$w_1(x_1) = -\frac{x_1}{4}(\pi r)^2, \quad \tilde{w}_1(x_1) = -\frac{(1+v)x_1}{4}(\pi r)^2, \quad w_2(x_1) = -\frac{1}{4}\pi r. \tag{A.16}$$

Introducing these expressions into (2.18), (2.19), (2.20) and (2.13), one obtains to the leading order in r:

$$\left(\left(\left(\mathcal{E}_{,uuuu}^c \overset{1}{u}\right)\overset{1}{u}\right)\overset{1}{u}\right)\overset{1}{u} = \frac{9(1+v)}{2(1-v)}\pi^4 r^3, \quad \left(\left(\mathcal{E}_{,uuu}^c \overset{2}{u}\right)\overset{1}{u}\right)\overset{1}{u} = -\frac{2+3v+v^2}{2(1-v)}\pi^4 r^3,$$

$$\left((\mathrm{d}\mathcal{E}_{,uu}/\mathrm{d}\Lambda)^c \overset{1}{u}\right)\overset{1}{u} = -2(1+v)\pi^2 r, \quad \Lambda_2 = \frac{1}{4}(\pi r)^2 \tag{A.17}$$

thus providing an independent confirmation that the limit $\Lambda_2(r)/\Lambda_c(r) \to 3$ as $r \to 0$ is identical to the one found from the numerical calculations reported in Fig. 7.

(ii) Tension (critical mode $\mathcal{A}^1$, $\mathcal{S}^2$; critical wavenumber $n_c = 1$)

The asymptotic expressions given below correspond to the Blatz–Ko material under tension. These expressions are given up to the lowest nontrivial order in r required for the calculation of Λ_2, the post-bifurcation curvature at the critical point.

To calculate Λ_2, one starts again with the asymptotic expressions of the stretch ratios λ_i and $v_i(x_1)$ (the x_1-dependent part of the eigenmode $\overset{1}{u}$) at the critical point:

$$(\lambda_1)_c = 3^{-1/4}\left[1 - \frac{1}{2916}(\pi r)^2\right] + \mathrm{O}(r^4), \quad (\lambda_2)_c = 3^{3/4}\left[1 + \frac{1}{972}(\pi r)^2\right] + \mathrm{O}(r^4),$$

$$v_1(x_1) = \frac{x_1}{9\sqrt{2}}\pi r + \mathrm{O}(r^3). \quad v_2(x_1) = \sqrt{2} + \mathrm{O}(r^2). \tag{A.18}$$

The asymptotic expansions for $w_i(x_1)$, $\tilde{w}_1(x_1)$ (the x_1-dependent parts of $\overset{2}{u}$) are recorded next. For the calculations of Λ_2 in tension, the first two terms in the r-expansions of $w_i(x_1)$ are required

$$w_1(x_1) = 3^{1/4}\left[3x_1 - \frac{x_1^3}{486}(\pi r)^2\right], \quad \tilde{w}_1(x_1) = 3^{1/4}\frac{x_1}{81}(\pi r)^2, \quad w_2(x_1) = 3^{1/4}\left[-\frac{27}{\pi r} + \frac{x_1^2}{2}\pi r\right]. \tag{A.19}$$

Upon introduction of the above expressions into (2.18), (2.19), (2.20) and (2.13), one obtains to the leading order in r:

$$\left(\left(\left(\mathcal{E}^c_{,uuuu}\overset{1}{u}\right)\overset{1}{u}\right)\overset{1}{u}\right)\overset{1}{u} = \frac{25}{81\sqrt{3}}\pi^4 r^3, \quad \left(\left(\mathcal{E}^c_{,uuu}\overset{2}{u}\right)\overset{1}{u}\right)\overset{1}{u} = -\frac{4}{\sqrt{3}}\pi^2 r,$$

$$\left((\mathrm{d}\mathcal{E}_{,uu}/\mathrm{d}\Lambda)^c\overset{1}{u}\right)\overset{1}{u} = -\frac{3^{1/4}8}{81}\pi^2 r, \quad \Lambda_2 = \frac{3^{3/4}27}{2} \tag{A.20}$$

thus establishing with a different method that the limit $\Lambda_2(r)/\Lambda_c(r) \to -27/2(3^{1/2} - 3^{-1/4})$ as $r \to 0$ coincides with the one found in the numerical calculations reported in Fig. 8.

References

Blatz, P.J., Ko, W.L., 1962. Application of finite elastic theory to the deformation or rubbery materials. Trans. Soc. Rheol. 6, 223–251.

Budiansky, B., 1974. Theory of buckling and postbuckling behavior of elastic structures. Adv. Appl. Mech. 14, 1–65.

Gent, A.N., 1996. A new constitutive relation for rubber. Rubb. Chem. Technol. 69, 59–61.

Healey, T.J., 1988. A group-theoretic approach to computational bifurcation problems with symmetry. Comp. Meth. Appl. Mech. Engin. 67, 257–295.

Healey, T.J., Simpson, H.C., 1998. Global continuation in nonlinear elasticity. Arch. Rational Mech. Anal. 143, 1–28.

Hill, R., Hutchinson, J.W., 1975. Bifurcation phenomena in the plane tension test. J. Mech. Phys. Solids 23, 239–264.

Hutchinson, J.W., 1974. Plastic buckling. Adv. Appl. Mech. 14, 67–144.

Knowles, J.K., Sternberg, E., 1975. On the ellipticity of the equations of nonlinear elastostatics for a special material. J. Elasticity 5, 341–361.

Koiter, W.T., (1945). On the stability of elastic equilibrium. (Delft Univ. Thesis in Dutch), NASA Tech. Transl. in 1967, TT F-10, 833.

Levinson, M., 1968. Stability of a compressed neo-Hookean rectangular parallelepiped. J. Mech. Phys. Solids 16, 875–900.

Ogden, R.W., 1984. Non-linear Elastic Deformations. Halsted Press, New York.

Rivlin, R., Sawyers, K., 1974. Stability of a compressed parallelepiped. J. Mech. Phys. Solids 23, 239–264.

Shanley, F.R., 1947. Inelastic column theory. J. Aero. Sci. 14, 261–267.

Triantafyllidis, N., Peek, R., 1992. On the stability and the worst imperfection shape in solids with nearly simultaneous eigenmodes. Int. J. Solids Struct. 29, 2281–2299.

Triantafyllidis, N. (2006). Unpublished work.

Young, N.J.B., 1976. Bifurcation phenomena in the plane compression test. J. Mech. Phys. Solids 24, 77–91.